Food Chemistry: X 25 (2025) 102151

Contents lists available at ScienceDirect

Food Chemistry: X

journal homepage: www.sciencedirect.com/journal/food-chemistry-x

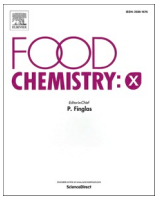

Sensitive ratiometric detection of Fumonisin B_1 using a reusable Ag-pSi SERS platform

Narsingh R. Nirala [a], Sudharsan Sadhasivam [b,c], Rohit Kumar Singh [a], Edward Sionov [b,*], Giorgi Shtenberg [a,*]

[a] Institute of Agricultural Engineering, ARO, Volcani Institute, Rishon LeZion, Israel
[b] Institute of Postharvest and Food Sciences, ARO, Volcani Institute, Rishon LeZion, Israel
[c] The Robert H. Smith Faculty of Agriculture, Food and Environment, Institute of Biochemistry, Food Science and Nutrition, The Hebrew University of Jerusalem, Rehovot 7610001, Israel

ARTICLE INFO

Keywords:
Aptamer
Food safety
Fumonisin B1
Porous silicon
SERS

ABSTRACT

Food and agricultural commodities endure consistent contamination by mycotoxins, low molecular weight fungal metabolites, which pose severe health implications to humans together with staggering economic losses. Herein, a ratiometric aptasensor was constructed using silver-coated porous silicon (Ag-pSi) used as an efficient surface-enhanced Raman scattering (SERS) substrate. The bioassay included direct detection of fumonisin B_1 (FB_1), an abundant and widespread contaminant, by a specific aptamer sequence immobilized on the porous transducer. The inherent surface void and pore morphology were physically optimized to achieve a sufficient SERS effect (enhancement factor $> 5 \times 10^7$). Under optimal conditions, the aptasensor exhibits high sensitivity, wide dynamic range, signal stability, selectivity and regeneration for consecutive FB_1 detection (0.05 ppb, 0.1–1000 ppb, RSD of 5.2 %, no interference with competing mycotoxins and eight regeneration cycles, respectively). The efficacy of the designed aptasensor was elucidated in various spiked matrices (maize, onion, wheat and milk) with averaged recovery values of 93.3–113.6 % and satisfactory consistency with HPLC data for representative foodstuffs. Overall, the resulting validation emphasizes the transducer's reliability and suitability for practical use, including on-site analysis.

1. Introduction

Food and agricultural commodities are constantly contaminated by various toxigenic molds that secrete poisonous chemical products formed as secondary metabolites (Hassan, Zareef, Xu, Li, & Chen, 2021). Among the various mycotoxin groups, fumonisin B1 (FB_1) is naturally generated by *Fusarium* species and is highly prevalent in maize, wheat, rice and soybean (Mirón-Mérida, Gong, & Goycoolea, 2021). According to the International Agency for Research on Cancer, FB_1 is considered a possible human carcinogen (group 2B) responsible for adverse health implications, such as gene mutation, kidney and liver poisoning, hematological and biochemical damages (Dong, Liu, Meng, Liu, & You, 2022). Due to the increased toxicological effects, the EU and the FDA have established a maximum tolerable daily intake of 2 μg/kg body weight (Gao et al., 2023). The ability to accurately detect and quantify contaminated food and feed at the early stage is of utmost importance to prevent potential health hazards to livestock and humans. Numerous methods are well facilitated for mycotoxins detection, including HPLC, LC-MS, ELISA and later flow assays (Logan et al., 2024). Although the high sensitivity and selectivity, most of these laboratory-based techniques are inadequate for *in situ* operation (intricate preparation procedures, exclusive equipment and personnel), while the portable techniques suffer from low throughput, limited stability and reproducibility, and most importantly an unappealing price tag for a single measurement (Gao et al., 2023; Huang et al., 2023).

Novel designs and sensing methods focus on exceeding these limitations to further improve and, at some point, replace the current analytical techniques. Among the emerging detection systems, optical-transduction is widely popular, *i.e.*, optical biosensors that demonstrate high sensitivity and selectivity, ease of detection, high-throughput analysis at on-site conditions, miniaturization toward lab-on-chip technology and reproducibility (Arshavsky-Graham, Massad-Ivanir, Segal, & Weiss, 2018). The recent rising star for ultrasensitive low molecular weight target molecule detection, operation-friendly and rapid

* Corresponding authors.
E-mail addresses: edwardsio@agri.gov.il (E. Sionov), giorgi@agri.gov.il (G. Shtenberg).

https://doi.org/10.1016/j.fochx.2024.102151
Received 7 June 2024; Received in revised form 27 December 2024; Accepted 30 December 2024
Available online 31 December 2024

multiplex constituents' assessment is the surface-enhanced Raman scattering (SERS) spectroscopy (Langer et al., 2020; Logan et al., 2024). The attractivity stems from the advancements in Raman signal amplification through electromagnetic and chemical enhancement mechanisms, rational design of the signal-generating platform and the efficiency of the affinity agent to capture its designated analyte. For example, Jiao et al. have shown a highly sensitive and reproducible multiplex mycotoxin SERS array based on gold nanoparticles-loaded inverse opal silica photonic crystal microsphere (Jiao et al., 2022). Three distinct Raman nanotags were utilized to code the target mycotoxins. The competitive immunoassay offered limit of detection (LOD) of 2.46, 0.20, and 68.98 pg/mL (parts per trillion) for OTA, FB_1, and DON, respectively, while achieving an impressive enhancement factor (EF) of 1.2×10^6. Other examples include SERS-based immunochromatographic assays (W. Zhang et al., 2020; Zheng et al., 2022), microfluidic systems (Pu, Xiao, & Sun, 2017; J. Zhang, Jiang, Li, Yuan, & Yang, 2023), and hybrid supports (Martinez & He, 2021; Mirón-Mérida et al., 2021), all of which excelled in terms of sensitivity, noninvasive and fingerprint information, while additional efforts should be devoted toward minimizing false-positive output of interfering residues in actual samples (Z. Wu, Pu, & Sun, 2021). In the last two decades, aptamers (artificial single-stranded oligonucleotides, DNA or RNA) have prevailed as an alternative capture probe to antibodies denoted due to their exceptional affinity and specificity, cost-effectiveness, ease of fabrication, durability and shelf-life stability (Mirón-Mérida et al., 2021). He et al. reported a bimodal (SERS and fluorometry) approach using competitive aptamer assay (detection aptamer labeled with Cy5 and complementary DNA-modified gold nanorods) (He, Wu, Cui, & Xu, 2020). In the presence of FB_1, the fluorophore-labeled composite was detached, resulting in recovered fluorescence and declined SERS signal. The assay offered LOD of 0.003 and 0.005 ppb (ng/mL) for SERS and fluorescence modes, respectively. Despite the massive exploration of numerous SERS-based platforms for mycotoxins detection, there is still an actual need for a robust, sensitive, cost-effective, stable and reusable pen-side sensing platform (Logan et al., 2024).

Herein, we present a direct sensing approach for the sensitive and selective detection of FB_1 in representative foodstuffs. Silver-coated porous silicon (Ag-pSi) was used as the SERS active substrate, renowned for its massive internal surface area, tunable pore size, ease of surface functionalization, and remarkable performance in various biosensing applications (Arshavsky-Graham et al., 2018; Khinevich et al., 2021; Nirala, Asiku, Dvir, & Shtenberg, 2022; Yang et al., 2024). Moreover, the produced substrates are compliant with any ratiometric SERS-based sensing, thus achieving a reliable quantitative detection method with pronounced reproducibility (Yan Wu et al., 2024). Initially, the experimental conditions were carefully optimized for an abundant SERS effect, including the inherent surface void and pore morphology, noble metal content and distribution. Then, the optimized Ag-pSi scaffold was labeled with 4-aminothiophenol (4-ATP, Raman marker) followed by anti-FB_1 aptamer modification to serve as the bio-recognition element that can comply with regenerating the scaffold for numerous consecutive sensing events while using the same portable scaffold. A ratiometric response evaluated the sensitivity, selectivity, stability and surface regeneration. Finally, the feasibility of near real-time assessment was investigated using foodstuff samples spiked or naturally contaminated with FB_1 in comparison with the traditional HPLC approach. Fig. 1 demonstrates the sensing concept upon target analyte capturing and detection, while the optical response gradually declined with augmented FB_1 content. The latter is associated with biocomplex formation and consequently signal masking, as previously shown (Muthukumar & Shtenberg, 2024; Yang et al., 2024; Yin et al., 2022; W. Zhang et al., 2020). Overall, this work holds significant promise for enhancing food safety measures and preventing the spread of minute contaminants, ultimately safeguarding public health.

2. Experimental section

2.1. Materials

P-type silicon wafers (B-doped, ⟨100⟩ oriented with an averaged resistivity of 1.0 mΩ cm) were obtained from Sil'tronix Silicon Technologies (France). Analytical grade buffers, methanol (MeOH), absolute ethanol (EtOH), 4-ATP, glutaraldehyde (GA, 50 %), FB_1, aflatoxin B1 (AFB_1), ochratoxin A (OTA), deoxynivalenol (DON), zearalenone (ZEN), silver nitrate ($AgNO_3$) and hydrofluoric acid (HF, 48 %) were purchased from Merck (Israel). Aptamer against FB_1 (αFB_1, 5'-NH_2-ATACCAGCTTATTCAATTAATCGCATTACCTTATACCAGCTTATTCAATTAC-3′) was purchased from Integrated DNA Technologies (IDT, Germany) (Frost, McKeague, Falcioni, & DeRosa, 2015).

2.2. Ag-pSi SERS platform fabrication

The pSi nanostructures were fabricated by two sequential anodization procedures used to remove the parasitic layer (also termed as a sacrificial layer) produced during the first etching step, as previously reported (Muthukumar & Shtenberg, 2023; Nirala et al., 2022). *Caution: HF is a highly toxic and corrosive substance; hence, physical contact should be evaded.* The wet etching conditions were 75, 300, and 526 mA cm^{-2} applied for 70, 18, and 10 s, respectively (resulting in scaffolds #1, #2 and #3). The freshly produced transducers were soaked in 1 mM $AgNO_3$ solution (50 % ethanol) for specific durations (0, 5, 10, and 30 min) to integrate AgNPs within the porous layer. The reduction was stopped after all surfaces were washed trice with ultrapure water and dried at 100 °C for 5 min. Then, all platforms were immersed in 1 μM ethanoic solution of 4-ATP for 60 min, resulting in 4-ATP/Ag-pSi surfaces. Subsequently, the optimal scaffold conditions were functionalized with

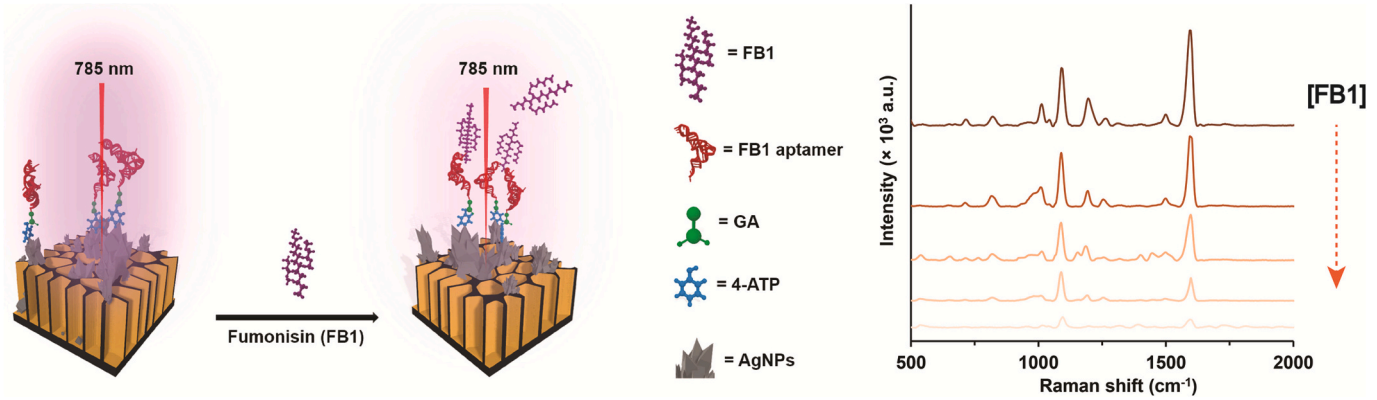

Fig. 1. Schematic representations of FB_1 (target analyte) capturing and detection using aptamer modified Ag-pSi SERS scaffold.

αFB_1 (10 μL at 1 μM) using 2.5 % (*v*/v) aqueous GA solution applied for 30 min and vigorously washed with ultrapure water to remove unbound residues (Sachin K Srivastava et al., 2015). The developed SERS platforms were stored under ambient conditions and immersed in a preheated Tris buffer (50 mM, pH 8.0, 70 °C) for 5 min prior to the intended analysis.

2.3. SERS-based detection of FB_1

An amount of 20 μL of different FB_1 concentrations (0.1 to 1000 ppb prepared in 10 % (v/v) MeOH in 50 mM HEPES buffer) were administered on αFB_1/4-ATP/Ag-pSi surfaces. The solutions were incubated at room temperature for 30 min to ensure sufficient recognition between the aptamers and the target molecules, thoroughly rinsed with HEPES buffer and dried using a low stream of nitrogen before optical inspection. The selectivity studies were similarly performed using different common interfering mycotoxins (*e.g.,* AFB_1, OTA, DON, and ZEN, 10 ppb each). Moreover, the stability and self-life were optically evaluated upon the target release using a preheated Tris buffer (50 mM, pH 8.0, 70 °C) applied for 5 min.

2.4. Foodstuff analysis

Various food samples were ground in a mixer mill (wheat, onion and maize). Following that, 10 mL of 10 % MeOH in HEPES buffer was used to suspend 5 g of the finely powdered foodstuff. The mixtures were stirred for 30 min prior to centrifugation (3000 ×*g* for 10 min) and syringe filtered (0.22 μm Milex®) to remove any insoluble matter. Moreover, bovine milk was defatted and used as an additional simulant of a complex matrix. Finally, the noted food matrices were spiked with 0.5, 5 and 50 ppb FB_1 using MeOH and assessed by the porous transducer.

2.5. Equipment and measurements

The resulting morphological features were characterized using a Carl Zeiss Ultra Plus HRSEM operated at 1 kV. The elemental composition was studied using a MIRA3 field-emission SEM microscope (TESCAN) coupled with EDX detector operated at 10 kV. Images were processed using Image J software. The open porosity values were calculated by Bruggeman effective medium approximation using the spectroscopic liquid infiltration method (SLIM) (Schwartz, Alvarez, & Sailor, 2007). Both Raman and SERS spectra were acquired using a portable spectrometer (QE*Pro* 650 by Ocean optics, FL, USA) with an input slit of 50 μm, equipped with 785 nm laser source (385 mW) while collecting three accumulations of 3 s exposure. Note: in order to minimize the spot-to-spot variation, all porous platforms were physically impregnated within a sample holder while assessing the same optical spot. The obtained spectra were normalized using OriginPro-2016 by asymmetric least squares smoothing and automatic baseline correction (Nirala et al., 2022).

The Ag-pSi SERS surface response was calculated as a ratiometric SERS intensity response located at 1598 cm^{-1} and defined as:

$$\text{Nor.Intensity}\ (\%) = \frac{I}{I_0} \times 100 \quad (1)$$

where, I represents the optical intensity response of the different solutions, while I_0 denotes the intensity value recorded at the baseline before the application of the studied solution onto the SERS platform (unmodified αFB1/4-ATP/Ag-pSi surface). Note: all reported data are reported as mean ± Std ($n \geq 3$).

2.6. Mycotoxin analysis

2.6.1. Fungal strain

Fumonisin-producing *Fusarium proliferatum* (*F. proliferatum*) strain YO3, isolated from red onion cv. Mata Hari, was used in this study. The strain was refreshed from −80 °C by subculturing on PDA plates and maintained at 28 °C before each experiment. Spores (macroconidia) were collected in sterile saline from cultures grown for 4 days and macroconidial suspension was adjusted to the required concentration by counting in a hemocytometer. Inoculum concentration was verified by plating on PDA plates for determination of CFU counts.

2.6.2. HPLC-based detection of FB_1 in food samples

Ten g of wheat grain, rice and oats samples were inoculated with 1 mL of 10^6 conidia/mL of *F. proliferatum*. Food samples treated with sterile water instead of fungal inoculum were used as negative controls. The samples were prepared in triplicate and incubated at 28 °C for 5 days. Then, the samples were freeze-dried and milled to a fine powder with a grain grinder. FB_1 content was analyzed by HPLC as described previously (Sadhasivam et al., 2022). Briefly, 2 g of the ground sample was extracted with 10 mL of the extraction solvent mixture (acetonitrile/methanol/water, 25:25:50, *v*/v). After agitation on an orbital shaker for 30 min, the samples were centrifuged at 8580 ×*g* for 15 min. A 2 mL aliquot of the supernatant was diluted with 8 mL phosphate buffered saline (PBS). Then, 10 mL of the diluted extract was passed through an immunoaffinity column (FumoniTest™ wide-bore, VICAM, Milford, MA, USA). The column was rinsed with 10 mL PBS and the toxin was eluted by passing 1 mL methanol followed by 1 mL water through the column. The eluate was evaporated to dryness under a nitrogen stream at 60 °C. The dried analytes were derivatized by solvent mixture of methanol (250 μL), 0.05 M sodium borate buffer (250 μL), sodium cyanide (125 μL) and 2,3-naphthalenedicarboxaldehyde (NDA, 125 μL). The mixture was allowed to react for 20 min at 60 °C in a water bath and then cooled down to room temperature. Then 250 μL of 0.05 M phosphate buffer (pH 7.4)/acetonitrile (40:60, v/v) was added to the mixture. The derivatized samples were filtered through a 0.22 μm PTFE filter and quantitatively analyzed by injection of 20 μL into a reversed phase HPLC/UHPLC system (Waters ACQUITY Arc, Milford, MA, USA) with an isocratic mobile phase consisting of 0.1 M sodium phosphate monobasic salt adjusted to pH 3.3 with orthophosphoric acid/methanol (230:770, v/v) at a flow rate of 1 mL/min through a Kinetex 3.5 μm XB-C18 (150 × 4.6 mm) column (Phenomenex). The column temperature was 30 °C. The noncontaminated food samples (wheat grain, rice and oats) were spiked with different concentrations (0.025, 0.05, 0.1, 0.5, 2 μg/g) of the mycotoxin FB_1 standard solution to construct the calibration curves. The FB_1 peak was detected with a fluorescence detector (Ex/Em at 420/500 nm) and quantified by comparing with the calibration curves of the mycotoxin standard. Similar solutions were assessed by the porous transducer.

3. Results and discussion

3.1. Ag-pSi nanostructures' topology and optical characteristics

The structural properties of noble metal-decorated SERS scaffolds are crucial for efficient sensing capabilities, such as optical performance and sensitivity threshold (Khinevich et al., 2021). Hence, the intrinsic features such as metal-dielectric scaffold pore diameter, thin layer thickness, open porosity, noble metal content, distribution on the pSi nanostructure and EF, were thoroughly evaluated. Three different current densities were used to construct various morphologies, mainly altered in their pore diameter and unchanged in the overall porous layer thickness. The latter was fixed at optimal penetration depth for porous SERS transducer based on previous reports (Giorgis et al., 2008; Nirala et al., 2022), while the former offered different substances load impregnation. HR-SEM images of the different porous scaffolds reveal the morphological features of open pores with averaged diameters of 32 ± 10, 52 ± 11 and 68 ± 13 nm for scaffolds #1, #2 and #3, respectively, see Fig. 2a, f, k (the pores size distribution is shown in Fig. S1). A uniform layer of un-branched channels with a characteristic thickness of

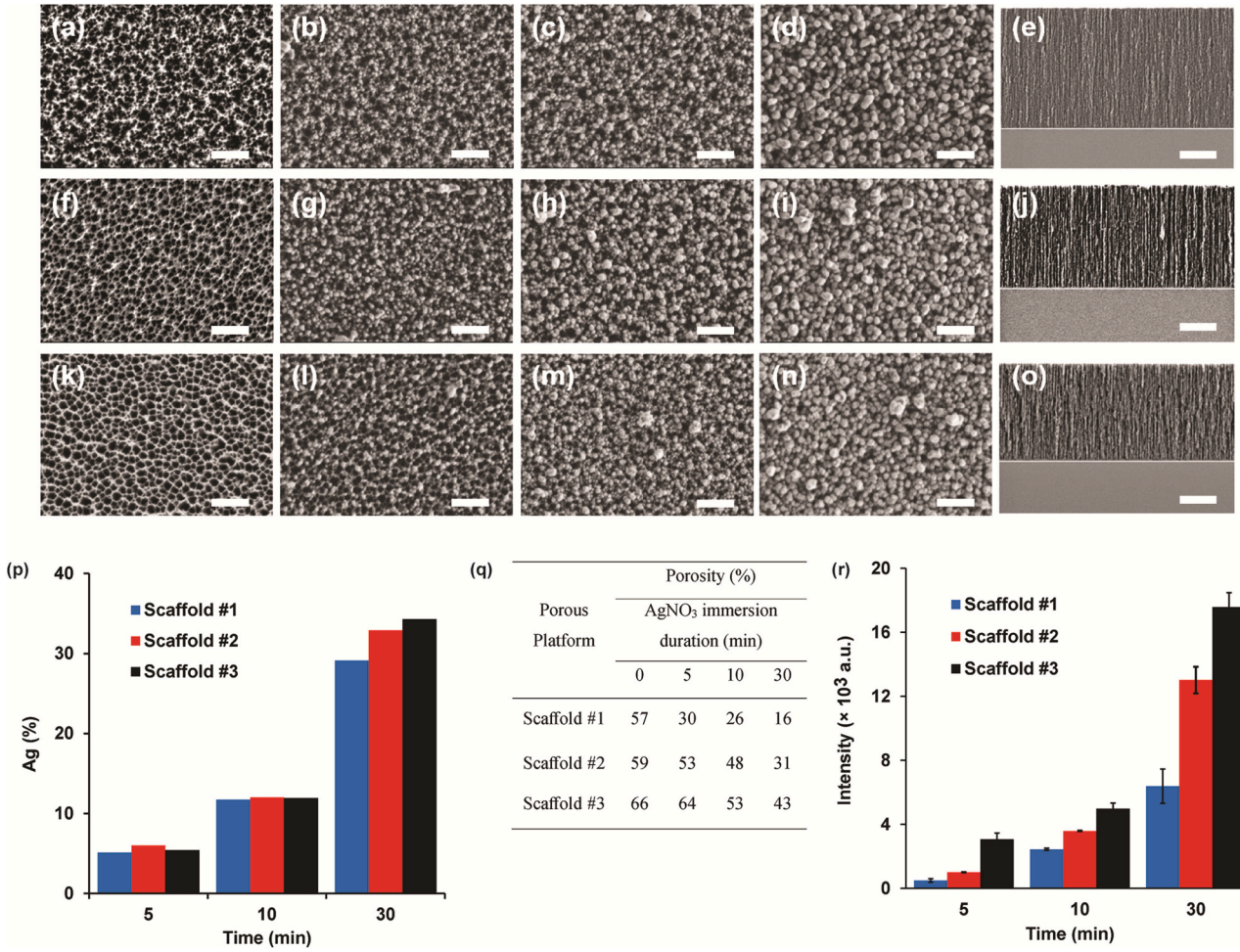

Porous Platform	Porosity (%) AgNO₃ immersion duration (min)			
	0	5	10	30
Scaffold #1	57	30	26	16
Scaffold #2	59	53	48	31
Scaffold #3	66	64	53	43

Fig. 2. HR-SEM images of the different porous scaffolds upon immersion plating with $AgNO_3$. Top row images of scaffold #1, middle row images of scaffold #2 and bottom row images are scaffold #3 (corresponding to wet etching conditions of 75, 300, and 526 mA cm^{-2} applied on bulk Si wafer for 70, 18, and 10 s, respectively). The immersion periods are (a, f, k) 0 min, (b, g, l) 5 min, (c, h, m) 10 min and (d, i, n) 30 min. Cross-sectional images (e) scaffold #1, (j) scaffold #2 and (o) scaffold #3. The scale bars are 300 nm and 1 μm for top and cross-sectional images, respectively. (p). EDX analysis of silver distribution. (q) Inherent porosities calculated by SLIM approach. (r) The corresponding SERS intensities of different 4-ATP/Ag-pSi scaffolds produced at different immersion periods. The intensified C=C stretching mode recorded at 1598 cm^{-1} was used for the assessment.

2.99 ± 0.31 μm was shown for all structures, see Fig. 2e, j, o. Immediately, the freshly anodized scaffolds were chemically oxidized in the presence of 1 mM $AgNO_3$ at various durations (0, 5, 10 and 30 min) to integrate noble metal nanoparticles on the thin films (Liu, Cheng, & Cui, 2014). The AgNPs distribution and size are dominated by redox-synthesis duration. Indeed, the HR-SEM images visualized augmented AgNPs dimensions upon elongated periods (for instance Fig. 2b, c, d), while insignificant differences in silver load were shown between similar dipping durations (Fig. 2d, i, n). It is to be mentioned that all studied surfaces produced relatively homogeneous silver coverage upon the noted distribution without incidences of silver agglomerates. To further complement the noble metal content coverage on the different Ag-pSi scaffolds, elemental analysis was performed using an EDX detector coupled to HR-SEM. Fig. 2p depicts that the atomic silver content increased profoundly upon elongated immersion periods for all analyzed scaffolds, in agreement with previous studies (Muthukumar & Shtenberg, 2023; Nirala et al., 2022). The only silver load deviation was obtained at 30 min of silver-plating that preferred larger pore width. These conditions presented atomic content of 29.1 ± 0.5, 32.7 ± 0.7 and 35.7 ± 1.9 % of for scaffolds #1, #2 and #3, respectively. Next, the open porosity values were calculated by Bruggeman effective medium approximation using SLIM. The approach utilizes the known refractive indexes of liquids infiltrating the porous void that alternate the interference components of the reflectance spectra. The attained data revealed a decrease in the open porosities with pores clogging at elongated immersion periods (Fig. 2q). In addition, the overall porosity was proportional to the anodization conditions, favoring higher current densities that generated increased porous voids. These results are in agreement with previous reports, exhibiting that the resulting SERS substrate based on a metal-coated anisotropic scaffold is formed by a rapid, straightforward and cost-effective method (Chursanova et al., 2010; Han et al., 2023; Khinevich et al., 2021).

The optical performances of the different SERS active substrates were investigated under controlled conditions using 1 μM ethanoic solution of 4-ATP (Raman tag) on the Ag-pSi. Fig. S2 shows a representative SERS spectrum of 4-ATP/Ag-pSi with the characteristic fingerprints of five major peaks (located at 824, 1089, 1194, 1243 and 1598 cm^{-1}) that are ascribed to the benzene ring and its functional groups. Table S1 reviews the attained peak positions with the chemical and vibrational assignments (Hu, Wang, Wang, & Dong, 2007; Osawa, Matsuda, Yoshii, & Uchida, 1994). Thereafter, the intensified C=C stretching mode recorded at 1598 cm^{-1} was used for the assessment. Fig. 2r depicts the corresponding SERS intensities of 4-ATP/Ag-pSi scaffolds produced at different immersion periods. A similar trend is shown for all studied scaffolds, in which the intensity rises in correlation to metal content growth. The wider pores of scaffold #3 outperformed other substrates

while presenting intensified values. For example, the SERS intensities obtained at 30 min of silver-plating were 6388 ± 1065, 13,023 ± 831 and 17,583 ± 900 a.u. for scaffold #1, #2 and #3, respectively. The attained increase is attributed to the physical features of the pSi-based SERS substrate, offering surface topology control of the generated local electric field between metal crystals faces (hot spots) needed for intensified SERS activity (Agafilushkina et al., 2020; Ge et al., 2020; Muthukumar & Shtenberg, 2023; Nirala et al., 2022). At this point, the amplified SERS output was compared with similar silver treatment conducted on a planar Si surface. Briefly, the bulk Si wafer was pre-treated with 36 % *v*/v ethanolic HF solution for 2 min without applying the electrochemical anodization procedure, thus receiving reductive species of silicon hydride (Liu et al., 2014). Immediately, the mono-crystalline Si substrate was soaked in 1 mM $AgNO_3$ for 30 min, followed by similar 4-ATP modification. Fig. S2 shows a representative SERS spectrum of 4-ATP/Ag-Si (non-anodized flat platform) with similar characteristic peaks. The intensified C═C stretching mode recorded at 1598 cm^{-1} presented values of 355 ± 170 a.u. that are 50-fold lower than a similarly treated porous scaffold #3 (Fig. S2, inset). This result strengthens the importance of the structural properties of noble metal-decorated SERS substrate to generate a proficient signal, in agreement with previous reports (Agafilushkina et al., 2020; Chursanova et al., 2010; Giorgis et al., 2008; Muthukumar & Shtenberg, 2023). Finally, the optical performance of the constructed SERS scaffolds was assessed through EF calculation. The scattered radiation proportion between SERS substrate intensity was compared with normal Raman signal attained from metal-free porous Si support using 4-ATP at 1 μM and 100 mM, respectively (Khinevich et al., 2021). The calculated EF were 3.9 × 10^7, 4.9 × 10^7 and 5.4 × 10^7 for scaffold #1, #2 and #3, correspondingly, see Supplementary Information. Thus, considering the intensified SERS performance, scaffold #3 soaked in 1 mM $AgNO_3$ for 30 min was chosen as the optimal SERS active substrate for all subsequent assessments.

3.2. Sensitivity, selectivity and homogeneity of SERS-based aptasensor

The optimized Ag-pSi scaffold was modified with an anti FB_1 aptamer to serve as a biorecognition element against the target molecule, resulting in αFB_1/4-ATP/Ag-pSi surface. Subsequently, a comprehensive dynamic response was acquired upon direct detection of the solid support. Briefly, 20 μL of different FB_1 concentrations (0 to 1000

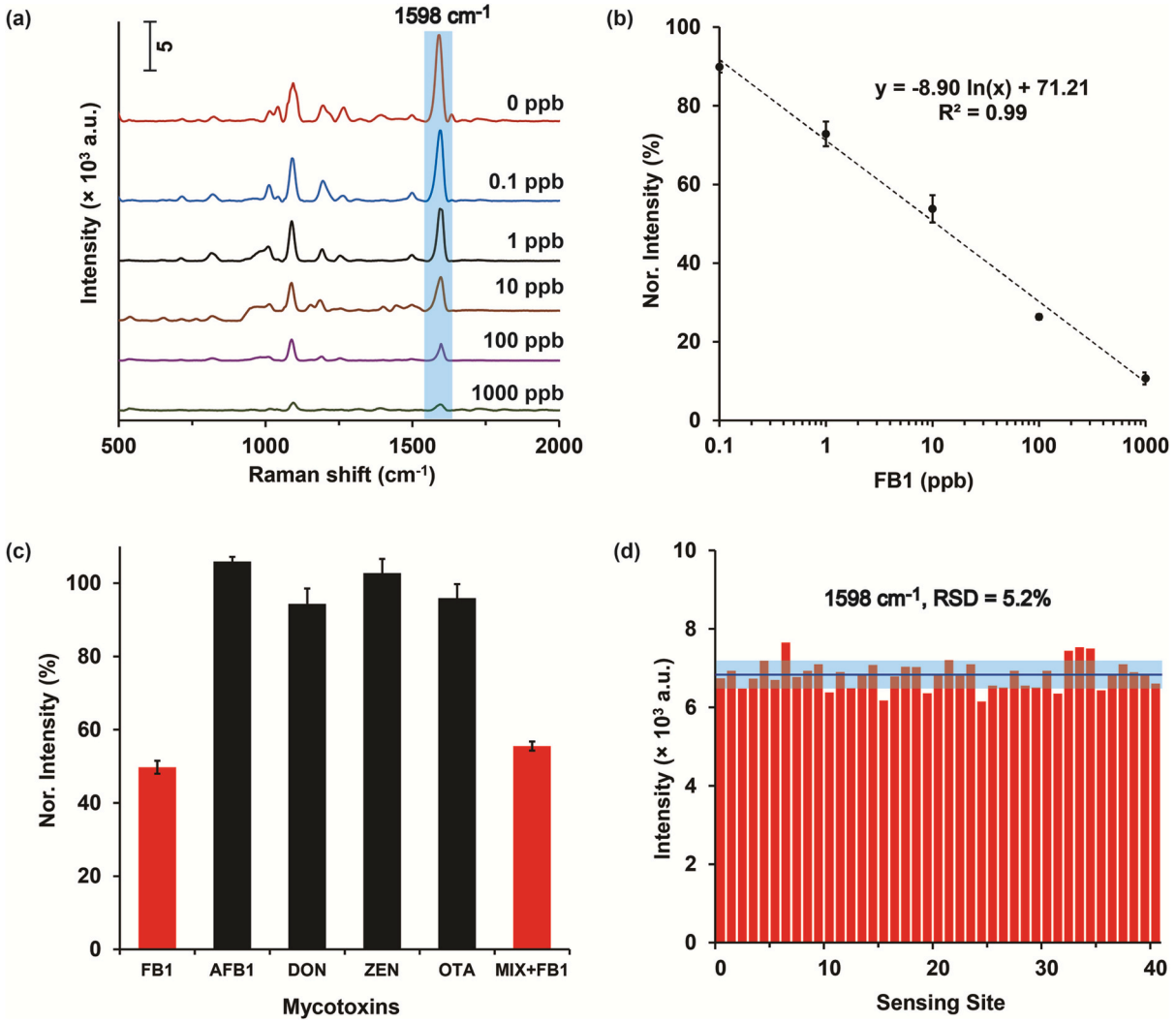

Fig. 3. (a) Representative SERS spectra of αFB_1/4-ATP/Ag-pSi surfaces toward various FB_1 concentrations (0 to 1000 ppb). (b) Corresponding calibration curve using normalized SERS intensity obtained at 1598 cm^{-1}. The normalization was performed with respect to the intensity value recorded prior to any interaction (unreacted of αFB_1/4-ATP/Ag-pSi surface). (c) Selectivity study using competing mycotoxins (all targets were fixed at a final concentration of 10 ppb). Note: mix stands for a mixture of AFB_1, ZEN, DON and OTA. (d) SERS signal distribution of 40 randomly recorded sensing spots using 1598 cm^{-1} peak. The average line is plotted with a blue line and the navy regions indicate the intensity variation (±5.2 %).

ppb) were administered on the SERS substrates, allowed to interact for 30 min, washed and dried prior to optical assessment. Fig. 3a shows representative SERS spectra of the characteristic fingerprint using a 4-ATP molecule as a Raman reporting tag. The optical response proportionally decreased with increased FB_1 content and thus inhibited the inherent SERS signal of αFB_1/4-ATP/Ag-pSi surface. Next, a calibration curve was constructed to establish a quantitative relationship between the optical response and the mycotoxin concentration using ratiometric SERS response of normalized intensities (Fig. 3b). Note: the attained peak intensities measured at 1598 cm^{-1} were normalized to the intensity of the unreacted scaffold (prior to any substance interaction). The fitted regression equation was Normalized Intensity $= -8.90 \times \mathrm{Ln}(C_{FB1}) + 71.21$, with a regression coefficient of 0.99. The optical response declined on a logarithmic correlation while assessing the dynamic range of FB_1. Similar optical output was previously shown for the direct assessment of a biorecognition event (Muthukumar & Shtenberg, 2023, 2024; Sachin K. Srivastava et al., 2014). The calculated LOD was 0.05 ppb using three standard deviations of the control sample (that omitted FB_1 from the bioassay) proportion to the fitting curve slope. The attained value is well below the threshold levels set by the current EU legislation and Codex standards for food and feed ($\leq$ 2000 ppb) (Terciolo et al., 2019; Yongning Wu, 2014). Similarly, the limit of quantification (LOQ) and coefficient of variation (CV) were computed, revealing 0.12 ppb and 5.2 %, respectively, Table S2 (Cámara, Bornancini, Cabrera, Ortega, & Yudi, 2010; Wang, Tan, Zhao, Liu, & Li, 2024).

Next, the selectivity of the bioassay was thoroughly studied using commonly known interfering mycotoxins (*i.e.,* AFB_1, ZEN, DON and OTA). The selectivity assessment is a crucial feature needed for innate performance evaluation in complex matrices applicable to real-life practices. The final concentration of all examined mycotoxins was fixed to 10 ppb that were similarly applied on the solid support for sufficient biorecognition by the immobilized αFB_1 and were optically assessed thereafter. Fig. 3c depicts the normalized optical response of the noted mycotoxins with respect to the FB_1 (used as a control). Negligible interferences for all competing mycotoxins were shown, while the condition that included the target analyte was equivalent to the response of only FB_1 (55.5 $\pm$ 1.2 and 49.7 $\pm$ 1.8 %, respectively). Therefore, the obtained results strongly support satisfactory selectivity using the unique binding affinity of αFB_1 toward accurate FB_1 detection without conceding the optical performances. Another critical parameter while assessing the collected intensity of the solid support substrate would be the efficiency of reproducing a homogenous signal across the SERS surface. Fig. 3d depicts the signal distribution of 40 randomly recorded sensing spots using the intensive peak located at 1598 cm^{-1}. The average intensity of αFB_1/4-ATP/Ag-pSi surface was 6826 $\pm$ 353 a.u. while the calculated relative standard deviation (RSD) was 5.2 %. The sufficient reproducibility of the constructed aptasensor outperformed previously reported pSi-based SERS active substrates that included numerous structural compositions combined with conventional and affordable metals (Khinevich et al., 2021).

3.3. SERS platform regeneration

One of the favorable advantages of using aptamers for any bioassay or biosensing scheme is their reversible denaturation feature that is amenable to consecutive sensing events (Arshavsky-Graham et al., 2020; Mirón-Mérida et al., 2021). The regeneration process will include the release of the target molecule upon aptamer's unfolding process (*e.g.,* preheated solution, regeneration buffer, *etc.*), thus resulting in a recyclable substrate's surface. The reversible nature of the developed SERS platform was thoroughly elucidated. Fig. 4 presents the normalized intensity values (ratiometric response) upon eight regeneration cycles with respect to the control sample (first sensing event). Despite mild alterations in the obtained regeneration values (<6.7 %), all sensing cycles fluctuated around the normalized value of the control sample

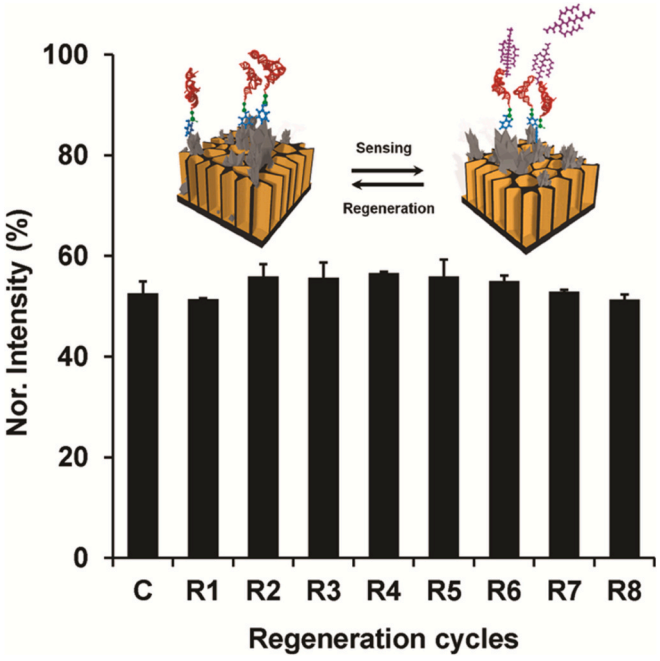

Fig. 4. SERS substrate reusability assessment. The αFB_1/4-ATP/Ag-pSi surface was recycled using preheated Tris buffer (50 mM, pH 8.0, 70 °C) that was applied for 5 min on the substrate. All sensing events monitored 10 ppb FB_1.

(52.6 $\pm$ 2.3 %). These findings demonstrate that the developed SERS substrate remains effective for up to eight regeneration cycles. The restoration capability ensures its long-term use and practicality in various applications. Table 1 compares the developed SERS-based assay with recent sensing and biosensing approaches for FB1 assessment. Although several platforms depicted enhanced sensitivities (lower LOD values), the presented SERS-based assay exhibited several profound advantages for practical use, such as direct target analyte detection, simplified and straightforward sensing protocol (sample drop-wash-measure), wide dynamic range, rapid assay duration and a generic sensing concept using aptamers as the biorecognition element. Moreover, the ratiometric design minimizes the need for internal standard addition (a supplementary inert Raman active molecule) and minimizes the effect of substrate feature fluctuations upon various fabrication processes (batch-to-batch variation). The substrate's ability to maintain a significant portion of its initial intensity after multiple regenerations enhances its sustainability and cost-effectiveness in comparison to other techniques. To the best of our knowledge the eight reuses of the sensing platform is the maximal regeneration cycles reported to date (Table 1). This means that the ability to reuse the transducer for numerous effective biorecognition events minimizes the price tag for a single measurement by 8-fold and surpasses other state-of-the-art techniques, hence indicating the novelty of the produced pen-side sensing platform. Overall, the evaluation highlights the resilience and practical applicability of the portable SERS substrate for reliable and prolonged use while assessing minute FB1 residues.

3.4. Detection of FB_1 in real foodstuff

The efficacy of the designed aptasensor was elucidated using spiked conditions in various foods. All samples were spiked with standard solutions of 0.5, 5.0 and 50 ppb of FB_1 and were optically evaluated. Table 2 summarizes the detected values using the regression relationship of the calibration curve. The calculated recovery values of maize, onion and wheat were between 93.3 % to 109.8 %. Moreover, defatted milk was used as an additional complex matrix example that entails numerous constituents (*e.g.,* fat globules, white cells, proteins, nutrients

Table 1
Comparison of the developed SERS-based assay with recent sensing and biosensing approaches for target molecule assessment.

Detection methods	Receptor	Transducer	Linear range (ppb)	LOD (ppb)	Assay Duration (min)	Portability	Reusable (regeneration cycles)	SERS EF ($\times 10^6$)	Refs.
Colorimetry	Antibody	AuNP	3–25	12.5	120	–	–	–	(Chen, Liang, Zhang, Leng, & Xiong, 2018)
Colorimetry	Aptamer	Microplate	0.5 -300	0.3	110	–	–	–	(Tao, Zhou, Li, & Wang, 2020)
Colorimetry/ LSPR	Antibody	Microplate	0.1–500	0.1/ 0.06	100	–	–	–	(Zhou et al., 2024)
Fluorescence	Antibody	Glass slide	17.3–79.6	11.1	220	–	–	–	(Peltomaa et al., 2017)
Fluorescence	Antibody	Microplate	0.41–100	0.483	120	–	–	–	(Huang et al., 2023)
Electrochemistry	Antibody	Screen-printed carbon electrode	200–45,000	4.2	40	–	–	–	(Lu, Seenivasan, Wang, Yu, & Gunasekaran, 2016)
Electrochemistry	Aptamer	AuNR	0.001-100	0.00026	15	–	+ (5)	–	(Wei, Xin, Feng, & Liu, 2020)
Fluorescence/ SERS	Aptamer	Pt-AuNR	0.01–0.25/ 0.01–0.5	0.005/ 0.003	45	–	–	–	(He et al., 2020)
SERS	Antibody	Graphene oxide Au-nano film	0.0046–10	0.000529	20	–	–	354	(Zheng et al., 2022)
SERS	Antibody	AuNPs- silica inverse opal	0.001–10	0.00026	90	–	–	1.2	(Jiao et al., 2022)
SERS	Antibody	Nitrocellulose membrane	0.4–300	0.26	20	+	–	–	(W. Zhang et al., 2020)
SERS	Aptamer	Ag-pSi	0.1–1000	0.05	30	+	+ (8)	54	This work

Table 2
Accuracy of the SERS-based platform to quantify spiked FB_1 in various foodstuffs.

Real samples	Detected [a] (ppb)	Recovery (%)	Detected [b] (ppb)	Recovery (%)	Detected [c] (ppb)	Recovery (%)
Maize	0.49 ± 0.08	97.6	4.90 ± 0.58	98.0	53.18 ± 3.52	106.4
Onion	0.47 ± 0.07	93.4	4.79 ± 0.35	95.7	54.88 ± 3.80	109.8
Wheat	0.47 ± 0.11	93.3	4.97 ± 0.35	99.3	53.72 ± 1.66	107.4
Defatted Milk	0.49 ± 0.07	98.1	5.26 ± 0.47	105.3	56.82 ± 0.37	113.6

Note: Spiked conditions were 0.5[a], 5.0[b] and 50[c] ppb of FB1.

and others) that may impede the sensing event. The attained recovery values found in milk were between 98.1 % to 113.6 %. More importantly, three foodstuffs (wheat, rice, and oats) were inoculated with *F. proliferatum*, allowed it to cultivate and secrete its secondary metabolites that were later assessed by the routine method of analytical chemistry using HPLC. Table 3 presents the comparative assessment of the aptasensor *vs* gold standard approach while depicting recoveries of 95.0, 99.8 and 114.3 % in wheat, rice and oats, respectively. The comparative study indicated acceptable accuracy of the developed bioassay to quantify minute toxins in different foodstuffs. The successful application of the developed SERS bioassay in analyzing real samples emphasizes its reliability and suitability for practical use, including on-site analysis. The ability to accurately detect and quantify contaminated food at the early stage is of utmost importance for ensuring food safety and preventing potential health hazards.

4. Conclusions

A ratiometric aptasensor was utilized for minute FB_1 residue assessment while employing a highly porous SERS substrate coupled with a specific DNA sequence. The efficient bioassay exhibited several profound advantages, such as a rapid (30 min), straightforward (sample drop-wash-measure), cost-effective and portable approach. Moreover, the direct sensing scheme offered high sensitivity, wide dynamic range, signal stability, selectivity and regeneration for consecutive FB_1 detection (0.05 ppb, 0.1–1000 ppb, RSD of 5.2 %, no interference with competing mycotoxins and eight regeneration cycles, respectively). The latter ability outperformed numerous state-of-the-art techniques, resulting in a price tag reduction for a single measurement by 8-fold. The practicality of real samples evaluation was in compliance with the gold standard approach (HPLC). Despite the high-throughput analysis deficiency, the developed framework is reusable and optically durable, thus demonstrating its potential applicability for point-of-care/site testing. Future research will tackle the noted limitation by extrapolating the rigid support design into an array format while detecting other hazardous toxins or low molecular weight contaminants with preserved analytical performances. Moreover, we will focus on additional improvements such as sample pretreatment, liquid handling and power supply for energy consumers to expand the potential for pen-side sensing.

Table 3
SERS platform and HPLC estimates of FB_1 detection in various foodstuffs.

Foodstuff	SERS (ppb)	HPLC (ppb)	Recovery (%)
Wheat	537 ± 12	565 ± 20	95.0
Rice	575 ± 24	576 ± 26	99.8
Oats	249 ± 44	218 ± 5	114.3

CRediT authorship contribution statement

Narsingh R. Nirala: Writing – original draft, Visualization, Validation, Methodology, Investigation, Formal analysis, Conceptualization. **Sudharsan Sadhasivam:** Writing – original draft, Validation, Methodology, Formal analysis. **Rohit Kumar Singh:** Validation, Methodology, Formal analysis. **Edward Sionov:** Writing – review & editing, Supervision, Project administration, Methodology, Funding acquisition. **Giorgi**

Shtenberg: Writing – review & editing, Visualization, Supervision, Resources, Project administration, Methodology, Funding acquisition.

Declaration of competing interest

The authors declare that they have no known competing financial interests or personal relationships that could have appeared to influence the work reported in this paper.

Acknowledgments

GS and ES gratefully appreciate the financial support from the Israeli Ministry of Agriculture (20-07-0013). GS acknowledges the JCA Charitable Foundation support. The authors are grateful to Dr. Ze'ev Schmilovitch for the assistance with the Raman setup.

Appendix A. Supplementary data

Supplementary data to this article can be found online at https://doi.org/10.1016/j.fochx.2024.102151.

Data availability

Data will be made available on request.

References

Agafilushkina, S. N., Žukovskaja, O., Dyakov, S. A., Weber, K., Sivakov, V., Popp, J., … Osminkina, L. A. (2020). Raman signal enhancement tunable by gold-covered porous silicon films with different morphology. *Sensors, 20*(19), 5634.

Arshavsky-Graham, S., Massad-Ivanir, N., Segal, E., & Weiss, S. (2018). Porous silicon-based photonic biosensors: Current status and emerging applications. *Analytical Chemistry, 91*(1), 441–467.

Arshavsky-Graham, S., Urmann, K., Salama, R., Massad-Ivanir, N., Walter, J.-G., Scheper, T., & Segal, E. (2020). Aptamers vs. antibodies as capture probes in optical porous silicon biosensors. *Analyst, 145*(14), 4991–5003.

Cámara, C. I., Bornancini, C. A., Cabrera, J. L., Ortega, M. G., & Yudi, L. M. (2010). Quantitative analysis of boldine alkaloid in natural extracts by cyclic voltammetry at a liquid–liquid interface and validation of the method by comparison with high performance liquid chromatography. *Talanta, 83*(2), 623–630.

Chen, X., Liang, Y., Zhang, W., Leng, Y., & Xiong, Y. (2018). A colorimetric immunoassay based on glucose oxidase-induced AuNP aggregation for the detection of fumonisin B1. *Talanta, 186*, 29–35.

Chursanova, M. V., Germash, L. P., Yukhymchuk, V. O., Dzhagan, V. M., Khodasevich, I. A., & Cojoc, D. (2010). Optimization of porous silicon preparation technology for SERS applications. *Applied Surface Science, 256*(11), 3369–3373.

Dong, N., Liu, D., Meng, S., Liu, S., & You, T. (2022). Tetrahedral DNA nanostructure-enabled electrochemical aptasensor for ultrasensitive detection of fumonisin B1 with extended dynamic range. *Sensors and Actuators, B: Chemical, 354*, Article 130984.

Frost, N. R., McKeague, M., Falcioni, D., & DeRosa, M. C. (2015). An in solution assay for interrogation of affinity and rational minimer design for small molecule-binding aptamers. *Analyst, 140*(19), 6643–6651.

Gao, Z., Luo, K., Zhu, Q., Peng, J., Liu, C., Wang, X., … Zhang, H. (2023). The natural occurrence, toxicity mechanisms and management strategies of Fumonisin B1:A review. *Environmental Pollution, 320*, Article 121065.

Ge, D., Wei, J., Ding, J., Zhang, J., Ma, C., Wang, M., … Zhu, S. (2020). Silver Nano-dendrite-plated porous silicon substrates formed by single-step electrochemical synthesis for surface-enhanced Raman scattering. *ACS Applied Nano Materials, 3*(3), 3011–3018.

Giorgis, F., Descrovi, E., Chiodoni, A., Froner, E., Scarpa, M., Venturello, A., & Geobaldo, F. (2008). Porous silicon as efficient surface enhanced Raman scattering (SERS) substrate. *Applied Surface Science, 254*(22), 7494–7497.

Han, S., Chen, C., Chen, C., Wu, L., Wu, X., Lu, C., … Hou, J. (2023). Coupling annealed silver nanoparticles with a porous silicon Bragg mirror SERS substrate and machine learning for rapid non-invasive disease diagnosis. *Analytica Chimica Acta, 1254*, Article 341116.

Hassan, M. M., Zareef, M., Xu, Y., Li, H., & Chen, Q. (2021). SERS based sensor for mycotoxins detection: Challenges and improvements. *Food Chemistry, 344*, Article 128652.

He, D., Wu, Z., Cui, B., & Xu, E. (2020). Aptamer and gold nanorod–based fumonisin B1 assay using both fluorometry and SERS. *Microchimica Acta, 187*(4), 215.

Hu, X., Wang, T., Wang, L., & Dong, S. (2007). Surface-enhanced Raman scattering of 4-Aminothiophenol self-assembled monolayers in Sandwich structure with nanoparticle shape dependence: Off-surface Plasmon resonance condition. *Journal of Physical Chemistry C, 111*(19), 6962–6969.

Huang, N., Sheng, W., Bai, D., Sun, M., Ren, L., Wang, S., Zhang, W., & Jin, Z. (2023). Multiplex bio-barcode based fluorometric immunoassay for simultaneous determination of zearalenone, fumonisin B1, ochratoxin A, and aflatoxin B1 in cereals. *Food Control, 150*, Article 109759.

Jiao, S., Liu, J., Sun, J., Chang, Y., Wang, S., Dai, S., … Li, J. (2022). A highly sensitive and reproducible multiplex mycotoxin SERS array based on AuNPs-loaded inverse opal silica photonic crystal microsphere. *Sensors and Actuators, B: Chemical, 355*, Article 131245.

Khinevich, N., Bandarenka, H., Zavatski, S., Girel, K., Tamulevičienė, A., Tamulevičius, T., & Tamulevičius, S. (2021). Porous silicon - A versatile platform for mass-production of ultrasensitive SERS-active substrates. *Microporous and Mesoporous Materials, 323*, Article 111204.

Langer, J., Jimenez de Aberasturi, D., Aizpurua, J., Alvarez-Puebla, R. A., Auguié, B., Baumberg, J. J., … Liz-Marzán, L. M. (2020). Present and future of surface-enhanced Raman scattering. *ACS Nano, 14*(1), 28–117.

Liu, X., Cheng, H., & Cui, P. (2014). Catalysis by silver nanoparticles/porous silicon for the reduction of nitroaromatics in the presence of sodium borohydride. *Applied Surface Science, 292*, 695–701.

Logan, N., Cao, C., Freitag, S., Haughey, S. A., Krska, R., & Elliott, C. T. (2024). *Advancing mycotoxin detection in food and feed: Novel insights from surface-enhanced Raman spectroscopy (SERS)* (p. 2309625). Mater: Adv.

Lu, L., Seenivasan, R., Wang, Y.-C., Yu, J.-H., & Gunasekaran, S. (2016). An electrochemical Immunosensor for rapid and sensitive detection of mycotoxins Fumonisin B1 and Deoxynivalenol. *Electrochimica Acta, 213*, 89–97.

Martinez, L., & He, L. (2021). Detection of mycotoxins in food using surface-enhanced Raman spectroscopy: A review. *ACS Applied Bio Materials, 4*(1), 295–310.

Mirón-Mérida, V. A., Gong, Y. Y., & Goycoolea, F. M. (2021). Aptamer-based detection of fumonisin B1: A critical review. *Analytica Chimica Acta, 1160*, Article 338395.

Muthukumar, D., & Shtenberg, G. (2023). SERS-based immunosensor for E. Coli contaminants detection in milk using silver-coated nanoporous silicon substrates. *Talanta, 254*, Article 124132.

Muthukumar, D., & Shtenberg, G. (2024). Quantitative detection of Staphylococcus aureus using aptamer-based bioassay coupled with porous Si SERS platform. *Journal of Science: Advanced Materials and Devices, 100690*.

Nirala, N. R., Asiku, J., Dvir, H., & Shtenberg, G. (2022). N-acetyl-β-d-glucosaminidase activity assay for monitoring insulin-dependent diabetes using ag-porous Si SERS platform. *Talanta, 239*, Article 123087.

Osawa, M., Matsuda, N., Yoshii, K., & Uchida, I. (1994). Charge transfer resonance Raman process in surface-enhanced Raman scattering from p-aminothiophenol adsorbed on silver: Herzberg-teller contribution. *The Journal of Physical Chemistry, 98*(48), 12702–12707.

Peltomaa, R., Benito-Peña, E., Barderas, R., Sauer, U., González Andrade, M., & Moreno-Bondi, M. C. (2017). Microarray-based immunoassay with synthetic Mimotopes for the detection of Fumonisin B1. *Analytical Chemistry, 89*(11), 6216–6223.

Pu, H., Xiao, W., & Sun, D.-W. (2017). SERS-microfluidic systems: A potential platform for rapid analysis of food contaminants. *Trends in Food Science and Technology, 70*, 114–126.

Sadhasivam, S., Marshi, R., Barda, O., Zakin, V., Britzi, M., Gamliel, A., & Sionov, E. (2022). Ensiling process and pomegranate peel extract as a natural additive in potential prevention of fungal and mycotoxin contamination in silage. *Toxicology Reports, 9*, 1557–1565.

Schwartz, M. P., Alvarez, S. D., & Sailor, M. J. (2007). Porous SiO2 interferometric biosensor for quantitative determination of protein interactions: Binding of protein A to immunoglobulins derived from different species. *Analytical Chemistry, 79*(1), 327–334.

Srivastava, S. K., Hamo, H. B., Kushmaro, A., Marks, R. S., Grüner, C., Rauschenbach, B., & Abdulhalim, I. (2015). Highly sensitive and specific detection of E. Coli by a SERS nanobiosensor chip utilizing metallic nanosculptured thin films. *Analyst, 140*(9), 3201–3209.

Srivastava, S. K., Shalabney, A., Khalaila, I., Grüner, C., Rauschenbach, B., & Abdulhalim, I. (2014). SERS biosensor using metallic Nano-sculptured thin films for the detection of endocrine disrupting compound biomarker Vitellogenin. *Small, 10*(17), 3579–3587.

Tao, Z., Zhou, Y., Li, X., & Wang, Z. (2020). Competitive HRP-linked colorimetric aptasensor for the detection of fumonisin B1 in food based on dual biotin-streptavidin interaction. *Biosensors, 10*(4), 31.

Terciolo, C., Bracarense, A. P., Souto, P. C. M. C., Cossalter, A.-M., Dopavogui, L., Loiseau, N., … Oswald, I. P. (2019). Fumonisins at doses below EU regulatory limits induce histological alterations in piglets. *Toxins, 11*(9), 548.

Wang, T., Tan, H.-S., Zhao, L.-X., Liu, M., & Li, S.-S. (2024). A novel ratiometric aptasensor based on SERS for accurate quantification of cardiac troponin I. *Sensors and Actuators, B: Chemical, 412*, Article 135804.

Wei, M., Xin, L., Feng, S., & Liu, Y. (2020). Simultaneous electrochemical determination of ochratoxin A and fumonisin B1 with an aptasensor based on the use of a Y-shaped DNA structure on gold nanorods. *Microchimica Acta, 187*(2), 102.

Wu, Y. (2014). General standard for contaminants and toxins in food and feed. *Codex stan*, 193–1995.

Wu, Y., Liu, J., Xu, R., Li, J., Fu, C., Shi, W., & Chen, J. (2024). Recent advances in ratiometric surface-enhanced Raman spectroscopy sensing strategies. *Microchemical Journal, 199*, Article 110127.

Wu, Z., Pu, H., & Sun, D.-W. (2021). Fingerprinting and tagging detection of mycotoxins in Agri-food products by surface-enhanced Raman spectroscopy: Principles and recent applications. *Trends in Food Science and Technology, 110*, 393–404.

Yang, J., Li, W., Li, H., Wang, X., Xu, K., Li, Q., … Li, J. (2024). *Highly sensitive microarray immunoassay for multiple mycotoxins on engineered 3D porous silicon SERS substrate with silver nanoparticle magnetron sputtering.* Chem: Anal.

Yin, L., You, T., El-Seedi, H. R., El-Garawani, I. M., Guo, Z., Zou, X., & Cai, J. (2022). Rapid and sensitive detection of zearalenone in corn using SERS-based lateral flow immunosensor. *Food Chemistry, 396*, Article 133707.

Zhang, J., Jiang, L., Li, H., Yuan, R., & Yang, X. (2023). Construction of a SERS platform for sensitive detection of aflatoxin B1 based on CRISPR strategy. *Food Chemistry, 415*, Article 135768.

Zhang, W., Tang, S., Jin, Y., Yang, C., He, L., Wang, J., & Chen, Y. (2020). Multiplex SERS-based lateral flow immunosensor for the detection of major mycotoxins in maize utilizing dual Raman labels and triple test lines. *Journal of Hazardous Materials, 393*, Article 122348.

Zheng, S., Wang, C., Li, J., Wang, W., Yu, Q., Wang, C., & Wang, S. (2022). Graphene oxide-based three-dimensional au nanofilm with high-density and controllable hotspots: A powerful film-type SERS tag for immunochromatographic analysis of multiple mycotoxins in complex samples. *Chemical Engineering Journal, 448*, Article 137760.

Zhou, Y., Li, Y., Tang, X., Li, H., Zhang, Q., Soo Park, K., & Li, P. (2024). A dual-signal output plasmonic sensor based on glucose oxidase-triggered etching of triangular silver nanoprism for sensitive detection of fumonisins. *Microchemical Journal, 196*, Article 109713.